Struct Multidisc Optim (2014) 49:185–197
DOI 10.1007/s00158-013-0982-x

RESEARCH PAPER

Numerical instabilities in level set topology optimization with the extended finite element method

David Makhija · Kurt Maute

Received: 14 March 2013 / Revised: 18 June 2013 / Accepted: 25 July 2013 / Published online: 21 August 2013

Abstract This paper studies level set topology optimization of structures predicting the structural response by the eXtended Finite Element Method (XFEM). In contrast to Ersatz material approaches, the XFEM represents the geometry in the mechanical model by crisp boundaries. The traditional XFEM approach augments the approximation of the state variable fields with a fixed set of enrichment functions. For complex material layouts with small geometric features, this strategy may result in interpolation errors and non-physical coupling between disconnected material domains. These defects can lead to numerical instabilities in the optimized material layout, similar to checker-board patterns found in density methods. In this paper, a generalized Heaviside enrichment strategy is presented that adapts the set of enrichment functions to the material layout and consistently interpolates the state variable fields, bypassing the limitations of the traditional approach. This XFEM formulation is embedded into a level set topology optimization framework and studied with "material-void" and "material-material" design problems, optimizing the compliance via a mathematical programming method. The numerical results suggest that the generalized formulation of the XFEM resolves numerical instabilities, but regularization techniques are still required to control the optimized geometry. It is observed that constraining the perimeter effectively eliminates the emergence of small geometric features. In contrast, smoothing the level set field does not provide a reliable geometry control but mainly improves the convergence rate of the optimization process.

Keywords Topology optimization · Level sets · Extended finite element method · Enrichment strategy · Checker-boarding · Regularization · Perimeter constraint

D. Makhija · K. Maute (✉)
Department of Aerospace Engineering,
University of Colorado at Boulder,
Boulder, CO 429 UCB, USA
e-mail: maute@colorado.edu

D. Makhija
Department of Mechanical Engineering,
University of Colorado,
Boulder, CO 80309-0427, USA
e-mail: makhijad@colorado.edu

1 Introduction

Topology optimization provides engineers with a powerful and systematic design tool for structural, thermal, fluid, and multi-disciplinary applications. Topology optimization methods aim at discovering the optimal geometry of a body and/or inclusions within a body for particular performance measures. For a given design domain, the geometry is defined by the spatial distribution of two or more material phases where one of the materials may represent void. Two general approaches are used to describe the material layout: a) at every point in the design domain the material phase is specified, or b) the volumes occupied by the individual material phases are defined via bounding surfaces.

Directly describing the material layout at every point in the design domain leads to a discrete optimization problem which is typically ill-posed and, in parametrized form, computationally costly to solve. Instead, the integer formulation is relaxed by introducing fictitious porous materials. Varying the density of the fictitious material provides a continuous transition between the individual phases. Topology approaches following this concept are called density methods. Interpolation methods define the physical properties of the porous material as function of the density. Implicit or

explicit penalty approaches are used to lessen the occurrence of intermediate densities. Global and local regularization techniques, such as perimeter constraints and sensitivity filters, mitigate the mesh-dependency of the optimization results. Two popular representatives of density methods include the homogenization method of Bendsøe and Kikuchi (1988) and the solid isotropic material with penalization (SIMP) method introduced by Bendsøe (1989) and Zhou and Rozvany (1991). For an introduction into density methods, the reader is referred to the text book by Bendsøe and Sigmund (2003). The review paper by Sigmund and Maute (2013) summarizes recent developments.

Density methods typically create fuzzy interfaces defined by intermediate densities or introduce stair-stepping type boundaries when the material distribution converges to the individual material phases, for example by using the projection methods of Guest (2009) and Wang et al. (2011). These boundary representations may complicate the application of design dependent boundary conditions, affect the accuracy of enforcing boundary conditions, and trigger non-physical responses of the structure such as premature yielding due to stress singularities, shown by Maute et al. (1998). While some of these issues can often be mitigated through mesh refinement and adaptive re-meshing, as proposed for example by Maute and Ramm (1995, 1997), the drawbacks of density methods have motivated increased research on topology optimization approaches that use a crisp description of the structural boundaries and material interfaces, in particular level set methods.

The level set method defines the interface between two material phases via the iso-contour of a higher dimensional function; usually via the zero level set contour. This approach can describe complex geometries and shape/topology changes on fixed meshes. The level set method was first proposed by Osher and Sethian (1988) and has been used in numerous applications, such as computer graphics, multi-phase flows, and image processing. The conceptual idea of using level sets for topology optimization can be traced back to the work by Haber and Bendsøe (1998) and de Ruiter and van Keulen (2000), and Sethian and Wiegmann (2000).

The work by Allaire et al. (2004) and Wang et al. (2003) provides the road map for the majority of today's level set topology optimization methods. The level set field is discretized by the same mesh used for predicting the physical response. The level set field is mapped onto the mechanical model using the Ersatz material method. The Ersatz material method interpolates physical properties of a fictitious material as a function of the local level set value, similar to density methods. The level set field is updated in the optimization process by solving the Hamilton-Jacobi equation. The velocity field that advects the level set field is constructed via shape sensitivities of a merit function. The reader is referred to Burger and Osher (2005) for details on level set topology optimization schemes that follow this road map. A recent review paper by van Dijk et al. (2013) provides a comprehensive overview of level set topology optimization. Sigmund and Maute (2012) discuss the commonalities and differences between level set and density methods.

Level set functions accommodate a crisp description of the boundaries and provide information about the surface normal direction and curvature. However, an Ersatz material approach smears the interface location across one or more cells/elements depending on the specifics of the mapping technique, and loses the crispness of the boundary definition. Hence, the Ersatz material approach and density methods lead to similar issues with regard to enforcing boundary conditions and predicting the physical response along the boundary.

To circumvent Ersatz material concepts, one can either generate repeatedly new meshes which align with the geometry described by the zero level set contour or use immersed boundary techniques. Generating an entirely new body-fitted mesh typically suffers from robustness and efficiency issues, particularly for three dimensional problems, and affects the convergence of the optimization process; see for example the studies by Schleupen et al. (2000) and Wilke et al. (2006). Locally adapting the mesh to conform to the updated geometry only partially mitigates these drawbacks. The Super-imposed Finite Element Method (SFEM) of Fish (1992) provides an interesting alternative to traditional mesh refinement techniques by superimposing the approximations of a non-body-fitted with a locally body-fitted mesh. Wang and Wang (2006b) use the SFEM for predicting the structural response within a level set method. Xia et al. (2012) follow a similar approach and refine a triangulated background mesh for intersected elements.

Among immersed boundary techniques, the eXtended Finite Element Method (XFEM) enjoys increasing popularity for solving problems with dynamically evolving boundaries and interface geometries. The XFEM can capture spatially discontinuous solutions of partial differential equations on fixed meshes. Rather than locally refining the mesh, the XFEM augments the standard finite element interpolation space by introducing additional shape functions to describe kinks or jumps in the field variables within an element. Similar to the SFEM, the physical field is described by the superposition of the standard and enriched shape functions. However, the XFEM provides greater flexibility in combining different types of shape functions and leads to a simpler implementation as all shape functions are defined on one fixed mesh. The theoretical basis of the XFEM is the "partition of unity method", originally introduced by Babuška and Melenk (1997). Subsequently, the XFEM was developed by Daux et al. (2000) to simulate crack

propagation. It has since been applied to a broad range of problems; for example Gerstenberger and Wall (2008) adopt an XFEM approach for fluid-structure interaction problems and Fries (2009) for multi-phase flows. A general overview of the XFEM is given by Fries and Belytschko (2010).

The XFEM is attractive for shape and level set based topology optimization methods because of its applicability to a broad range of engineering problems and its rigorous mathematical foundation. For the particular case of two material phases with one of them representing "void" and simple geometric configurations, additional enriched degrees of freedom do not need to be introduced. If in addition, the phase boundaries are traction free, the XFEM differs from the standard finite element method only with respect to the domain of integration. As the response does not need to be modeled in the "void" phase, the weak form of the governing equations is only integrated over the material phase in each element. This simplified version of the XFEM is applied to shape optimization by van Miegroet et al. (2005), Duysinx et al. (2006), and van Miegroet and Duysinx (2007). If the physical model specifies Dirichlet boundary conditions along phase boundaries, the XFEM needs to be augmented by stabilized Lagrange multiplier or penalty methods to enforce the boundary conditions. For example, Kreissl and Maute (2012) solve flow topology optimization problems by enforcing the stick boundary conditions along the fluid-solid interface via a stabilized Lagrange multiplier formulation. Note, the flow topology optimization problems considered by Kreissl and Maute (2012) model the response only in the fluid phase as the solid phase is considered "void".

Topology optimization of two-phase problems using the XFEM is considered by Wei et al. (2010) and Maute et al. (2011). Wei et al. (2010) optimize the topology of linear elastic structures by modeling the "void" phase with an auxiliary soft material, similar to an Ersatz material approach. The numerical examples studied by Wei et al. (2010) suggest that not enriching the shape functions in intersected elements is adequate to predict the structural response as long as the auxiliary phase is significantly softer than the material phase. While this simplification does not resolve the discontinuity in the strain field along phase boundaries, the resulting error in the interface forces is negligible for the problems considered by these authors. In this study we will show that for "material-material" and even for "material-void" problems improper enrichments may cause significant errors which adversely affect the optimization results.

Maute et al. (2011) discretize the phonon Boltzmann transport equations by the XFEM and optimize the thermal conductivity of nano-structured composites. For this class of problems, the physical response needs to be predicted accurately in both phases. Intersected elements are enriched by Heaviside functions that capture discontinuities in the phonon distribution along material interfaces. However, as we will show subsequently, the enrichment strategies used in the previous work on two-phase problems of Wei et al. (2010) and Maute et al. (2011) are insufficient to accurately model the response for complex geometries that frequently emerge in topology optimization. Furthermore, these enrichment strategies may lead to numerical instabilities similar to "checker-boarding" in density methods.

In this paper we present a generalized formulation of the XFEM that provides an efficient and versatile analysis framework for level set topology optimization on fixed meshes. Our approach is based on Heaviside enrichments and stabilized formulations to enforce Dirichlet-type boundary conditions. We present an enrichment strategy that eliminates the need for adaptive mesh refinement along phase boundaries and addresses shortcomings in standard enrichment procedures for complex geometries. This feature is particularly attractive for topology optimization as small geometric features often merge in the optimization process, rendering mesh adaptation strategies impractical. We illustrate with numerical examples the detrimental impact of standard enrichment approaches on the optimized material layout and show that numerical artifacts can be efficiently mitigated by the proposed enrichment strategy. This paper presents applications to structural design optimization using mathematical programming methods, but the proposed XFEM formulation is applicable to a broad range of design problems and can be combined with Hamilton-Jacobi update schemes.

The remainder of this paper is arranged as follows: Section 2 provides a brief summary of the level set topology optimization strategy used in this study. Section 3 presents the XFEM framework and introduces the proposed enrichment strategy. In Section 4 we study two numerical examples to illustrate the features of level set topology optimization using the XFEM.

2 Topology optimization framework

The design optimization problems considered in the current study are written as:

$$\min_{\mathbf{s}} \mathcal{F}(\mathbf{s}, \mathbf{u}(\mathbf{s})),$$
$$\text{s.t.} \begin{cases} \mathbf{s}, & \text{subject to design constraints } \mathcal{G}_j \leq 0, \\ \mathbf{u}, & \text{solves } \tilde{W} = 0 \text{ for a given } \mathbf{s}, \end{cases} \tag{1}$$

where $\mathbf{s}$ denotes the vector of design variables, $\mathbf{u}$ the vector of state variables for all phases, $\mathcal{F}$ the objective function, $\mathcal{G}_j$ the j-th design constraint, and $\tilde{W}$ the state equations in

weak form. In general, the objective and constraints depend on the optimization and state variables.

The optimization variables describe the level set function $\phi(\mathbf{s}, \mathbf{x})$, where $\mathbf{x}$ is the spatial coordinate. For a two-phase problem, the material layout is defined as follows:

$$\begin{cases} \phi(s(\mathbf{x})) < 0, & \forall\, \mathbf{x} \in \Omega_A, \\ \phi(s(\mathbf{x})) > 0, & \forall\, \mathbf{x} \in \Omega_B, \\ \phi(s(\mathbf{x})) = 0, & \forall\, \mathbf{x} \in \Gamma_{A,B}, \end{cases} \tag{2}$$

where Ω_A is the domain occupied by phase "A", and Ω_B is the domain occupied by phase "B". The interface between phase "A" and "B" is denoted by $\Gamma_{A,B}$ and corresponds to the zero level set contour.

Instead of following the approach of Wang et al. (2003) and Allaire et al. (2004) and updating the level set function via the solution of the Hamilton-Jacobi equation, here the parameters of the discretized level set function are defined as explicit functions of the optimization variables and the resulting parameter optimization problem is solved by a mathematical programming scheme. Explicit level set methods were previously studied, for example, by Wang and Wang (2006a), Luo et al. (2007), and (Pingen et al. 2010). The particular approach used here is described in detail by Kreissl and Maute (2011) and outlined below.

Directly treating nodal level set values as optimization parameters leads to localized sensitivities within a small band along the zero level set contour and adversely affects the convergence rate of the optimization process. The following linear filter is used to widen the zone of influence of the optimization variables and to improve the convergence rate:

$$\phi_i = \frac{\sum_{j=1}^{N} \max\left(0, (r - d_{ij}) s_j\right)}{\sum_{j=1}^{N} \max\left(0, (r - d_{ij})\right)}, \tag{3}$$

where N is the number of nodes in the discrete model, r will be referred to as the filter radius, and d_{ij} is the distance between the i-th node and the j-th node. Note, in contrast to similar filters in density methods, the above filter neither guarantees that the design converges as the mesh is refined nor provides a local size control; see, for example, Sigmund and Maute (2013). Therefore, the optimization problem is regularized by a perimeter constraint which Allaire et al. (2004), Maute et al. (2011) and van Dijk et al. (2012) show to be an efficient technique to globally control the geometry in level set methods. Alternative formulations using a fictitious interface energy have also been successfully applied to regularize the optimization problem; see Yamada et al. (2010).

3 Extended finite element formulation

Given a level set field, the response of the system is predicted by the XFEM. The zero level set contour is directly captured by the XFEM formulation; no additional mapping or projection schemes are needed to define the phase boundaries on the computational mesh. This section provides first a brief outline of the XFEM for static, linear elastic structural models in two dimensions. Second, we introduce a generalized enrichment strategy to accurately capture the behavior of geometrically complex material layouts. Finally, we discuss the enforcement of interface conditions along the phase boundaries. We note that the framework described below is applicable to a broad range of 2D/3D problems, such as nonlinear elasticity, incompressible and compressible flows, and heat transfer.

3.1 Governing equations

We consider the two-phase problem depicted in Fig. 1. The static equilibrium is governed by the following set of equations:

$$\begin{cases} -\nabla \cdot (\boldsymbol{\sigma}) = \mathbf{b} & \text{in } \Omega, \\ \mathbf{u} = \bar{\mathbf{u}} & \text{on } \Gamma_D, \\ \boldsymbol{\sigma} \cdot \mathbf{n} = \mathbf{f} & \text{on } \Gamma_N, \end{cases} \tag{4}$$

where $\mathbf{u}$ is the displacements vector, $\boldsymbol{\sigma}(\mathbf{u})$ the stress tensor, $\mathbf{b}$ the applied body forces, $\bar{\mathbf{u}}$ the prescribed displacements along Γ_D, and $\mathbf{f}$ denotes the external traction along Γ_N. Assuming infinitesimal strains and a linear elastic material behavior yields the following constitutive and kinematic models:

$$\boldsymbol{\sigma} = \mathbf{C} : \boldsymbol{\varepsilon}(\mathbf{u}), \tag{5}$$

$$\boldsymbol{\varepsilon} = \frac{1}{2}\left(\nabla \mathbf{u} + \nabla \mathbf{u}^T\right), \tag{6}$$

where $\mathbf{C}$ is the elasticity tensor and $\boldsymbol{\varepsilon}$ the strain tensor.

The weak form of the governing equations is obtained by multiplying the strong form (4) by a kinematically admissible test function, $\mathbf{v}$, and integrating the product over the

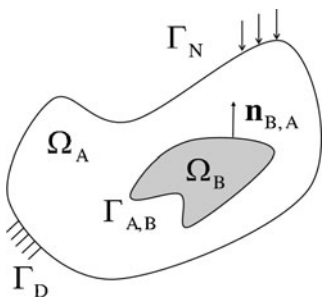

Fig. 1 Two-phase problem

domains Ω_A and Ω_B. Further integrating the divergence of the stress tensor by parts yields:

$$W = \int_{\Omega_A} \boldsymbol{\eta} : \boldsymbol{\sigma}\, d\Omega + \int_{\Omega_B} \boldsymbol{\eta} : \boldsymbol{\sigma}\, d\Omega - \int_{\Omega_A} \mathbf{v} \cdot \mathbf{b}\, d\Omega - \int_{\Omega_B} \mathbf{v} \cdot \mathbf{b}\, d\Omega - \int_{\Gamma_N} \mathbf{v} \cdot \mathbf{f}\, d\Gamma_N = 0, \tag{7}$$

where $\boldsymbol{\eta}$ is the strain tensor associated with the test function $\mathbf{v}$. Note in the derivation of the weak form (7) we assume that the displacements along the phase boundary $\Gamma_{A,B}$ are continuous and the sum of the boundary terms vanishes:

$$W_{A,B} = \int_{\Gamma_{A,B}} \mathbf{v}^{(A)} \cdot \left(\boldsymbol{\sigma}^{(A)} \cdot \mathbf{n}_{A,B}\right) d\Gamma + \int_{\Gamma_{B,A}} \mathbf{v}^{(B)} \cdot \left(\boldsymbol{\sigma}^{(B)} \cdot \mathbf{n}_{B,A}\right) d\Gamma = 0, \tag{8}$$

where $\mathbf{v}^{(A)}$ and $\boldsymbol{\sigma}^{(A)}$ exist in phase "A" and $\mathbf{v}^{(B)}$ and $\boldsymbol{\sigma}^{(B)}$ in phase "B". The normal vector $\mathbf{n}_{A,B}$ points from phase "A" to phase "B", and the normal vector $\mathbf{n}_{B,A}$ in the opposite direction.

For "material-void" problems, designs with free floating pieces of material may be generated in the course of the optimization process. A singular static equilibrium problem results as the rigid body motion of these pieces are not suppressed. In density methods and level set methods using Ersatz material, this issue is typically resolved by approximating the "void" phase with a soft material. Wei et al. (2010) follow a similar concept in their XFEM-based optimization approach. Alternatively, the problem can be resolved by adding soft springs between every material point and a fictitious support. The following additional stiffness term is added to the weak form of the governing equations (7) assuming phase "B" is the "void" phase:

$$W_k = W + \int_{\Omega_A} k\, \mathbf{v} \cdot \mathbf{u}\, d\Omega, \tag{9}$$

where k denotes the stiffness of the distributed system of springs. Note the spring stiffness in (9) can be implemented in lumped form. In contrast to modeling the "void" phase via a soft material, the proposed spring approach does not suffer from spurious load transfer through "void" regions and reduces the computational cost as elements in the "void domain" and their associated degrees of freedom can be omitted in the XFEM analysis.

In the XFEM, the weak form of the governing (7) is typically discretized by a structured mesh that is not aligned with the phase boundaries. As elements are intersected by the zero level set contour, the standard finite element shape functions are enriched such that they can capture discontinuities in the strain field along the phase boundaries. If the enrichment strategy does not inherently satisfy the interface conditions, the governing equations are augmented by additional interface constraints. Furthermore, the integrals over domains "A" and "B" in the weak form (7) are evaluated separately over the individual phases. To this end, intersected elements are typically triangulated and the integration is performed by Gauss quadrature for each triangle in 2D or tetrahedron in 3D. Here we will focus on the two key components of the proposed XFEM scheme, namely the enrichment strategy and the interface conditions.

3.1.1 Integration and enrichment strategy

In standard finite element methods a scalar field u is described by a superposition of interpolating functions scaled by their degree of freedom u_i,

$$u(x) = \sum_{i=1}^{n} N_i(x)\, u_i, \tag{10}$$

where N_i is the i-th interpolating or shape function, and n is the number of nodes used to interpolate u. The XFEM captures discontinuities by augmenting the standard interpolation with "enriched" shape functions and degrees of freedom. Depending on the type of discontinuity, so-called kink or step functions are used to enrich the interpolation; see, for example, Fries and Belytschko (2010). Kink-type enrichments are typically used to approximate the displacement field for elastic problems as they satisfy inherently the displacement continuity condition along the phase boundaries. However, these enrichment functions introduce spurious oscillations and lead to ill - conditioning of the finite element problem. To mitigate these issues, Fries (2008) introduces blending functions which, however, increase the complexity of the formulation and implementation.

To bypass these issues, we adopt a generalized version of the step enrichment of Hansbo and Hansbo (2004):

$$u(x) = \sum_{m=1}^{M} \left(H(-\phi) \sum_{i=1}^{n} N_i\, u^A_{i,m} + H(\phi) \sum_{i=1}^{n} N_i\, u^B_{i,m} \right), \tag{11}$$

where we refer to m as the enrichment level, M is the maximum number of enrichment levels used for each phase, $u^k_{i,m}$ is the degree of freedom at node i for phase k, and H is the Heaviside function,

$$H(z) = \begin{cases} 1 & z > 0, \\ 0 & z \leq 0. \end{cases} \tag{12}$$

Building upon the enrichment strategy of Terada et al. (2003), the enrichment formulation (11) considers multiple enrichment levels, m. In contrast to Terada et al. (2003), we interpret the enrichment levels node-wise rather than at an element level. The advantage of this concept will be discussed subsequently.

The need for this generalization is illustrated with a simple one-dimensional test problem, depicted in Fig. 2. Two

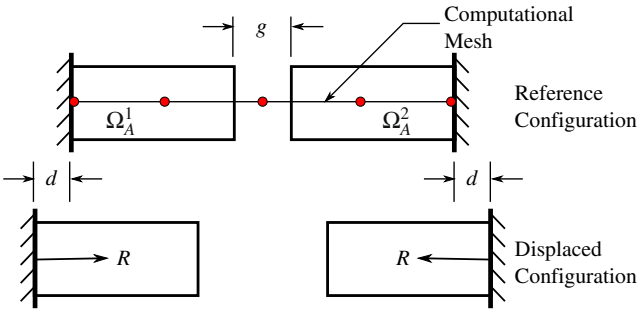

Fig. 2 One-dimensional example problem

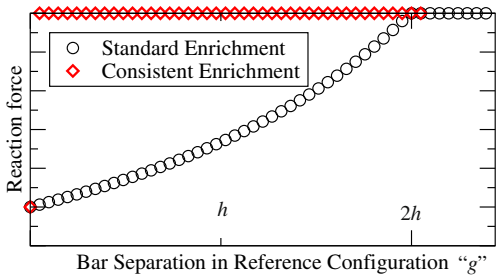

Fig. 4 Reaction force for consistent and standard enrichments over gap size, g

bars are fixed to a wall on opposite ends and the length of the gap between the bars is denoted by g. The fixed boundaries are displaced by d in opposite directions, forcing the bars to further separate. The reaction force R at the walls should be zero since the bars are not physically connected.

The bar problem is analyzed by the XFEM. The computational domain includes both bars (phase "A") and the gap in between (phase "B"). The domain is discretized with a regular mesh with an element length of $h = \Delta x$. The phase "A" interpolating functions for the standard enrichment are shown in Fig. 3. Note that the shape functions defined at the center node interpolates the displacements in both bars connected to this node when $g < 2h$. Phase "B" is void, and does not contribute to the weak form of the governing (7).

The reaction force, R, is plotted against the gap distance, g, in Fig. 4. A non-zero reaction force is obtained for a gap of $g < 2h$. A spurious coupling exists when the gap is contained within the elements connected to the center node. As we will show later, this spurious coupling leads to geometric artifacts when conventional XFEM strategies are used in level set topology optimization methods.

To remedy this issue, we check the shape functions defined at a given node over all elements connected to the node. If a shape function interpolates a state variable field in domains of identical phase that are not physically connected over the node's elements, additional shape functions are introduced and assigned different enrichment levels. This procedure leads to a generalized enrichment strategy where the displacement fields in disconnected domains of identical phase are approximated by different shape functions.

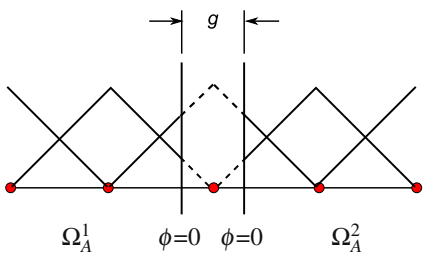

Fig. 3 Interpolation using standard Heaviside enrichment

Thus, the interpolation is consistent with the layout of the material phases. Note the connectivity of domains is only analyzed over the elements connected to the given node, but not globally over the entire mesh.

Figure 5 displays the interpolations of the generalized enrichment strategy. The two bars connected to the center node are interpolated by independent functions. The artificial coupling between the two bars introduced by the standard enrichment strategy is removed and the consistent enrichment recovers a reaction force of 0 for any gap distance $g > 0$.

The concept is easily generalized for two dimensions, but the number of possible enrichments increases. An element with a bi-linear interpolation of the level set field can be intersected no more than twice on a fixed mesh. The geometrically most complex configurations require a maximum of $M = 5$ enrichment levels. An example where the maximum number of enrichment levels is needed is depicted in Fig. 6; the shape functions defined at the center node interpolate the displacement field in five disconnected areas of phase "A". The numerical examples in Section 4 will illustrate that this feature is crucial to avoid artificial stiffening and the formation of artifacts in the optimization process.

Formally we write the state variable field interpolation (11) as a sum over several enrichment levels, m. However,

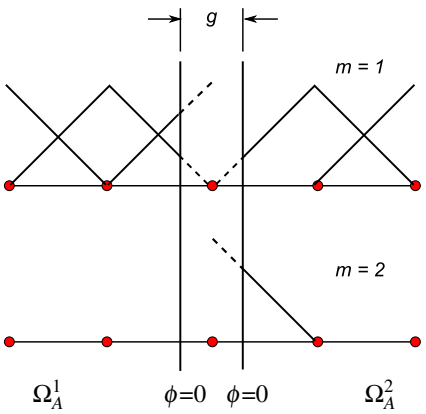

Fig. 5 Interpolation using the generalized (consistent) Heaviside enrichment

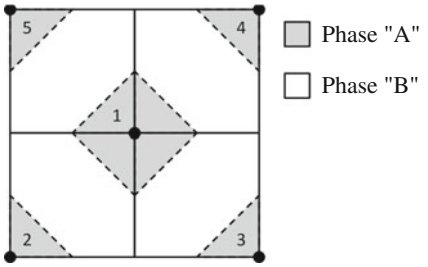

Fig. 6 Geometric configuration requiring five enrichment levels

the implementation of this approach can be greatly simplified as only one enrichment level will be active at any given point within an element for each node. The finite cover approach of Terada et al. (2003) similarly considers a "physical cover layer" which determines the active enrichment level, m, at a point within an element. However, assigning individual enrichment levels to the shape functions defined at nodes rather than to elements allows interpolating a state variable at a point by shape functions belonging to different enrichment levels. For example, consider the consistent enrichment of the one dimensional bar problem shown in Fig. 5. The displacements at points in the element right of the center node belonging to phase Ω_A^2 are interpolated by two shape functions that belong to different enrichment levels, namely $m = 1$ and $m = 2$. Note, in this formulation the total number of active interpolating functions always equals the number of nodes n, i.e. a single active interpolating function for each node.

One advantage of this implementation of the XFEM is that any type of shape function with local support can be used and only the Gauss point locations and the assembly process are modified. The Gauss points correspond to the quadrature rule for the decomposed triangle. The residual vector and Jacobian matrix of the discretized governing equations are assembled into the corresponding enrichment levels. Degrees of freedom that correspond to unused enrichment levels can be removed from the residual equations. We will show in Section 4 that several levels of enrichment are crucial in obtaining reasonable designs in topology optimization.

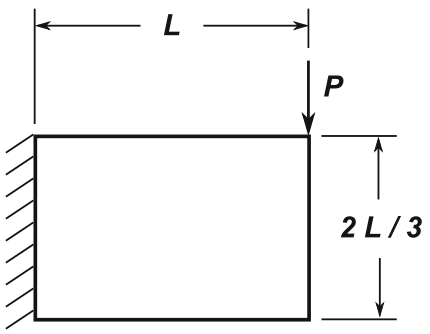

Fig. 7 Cantilevered beam problem

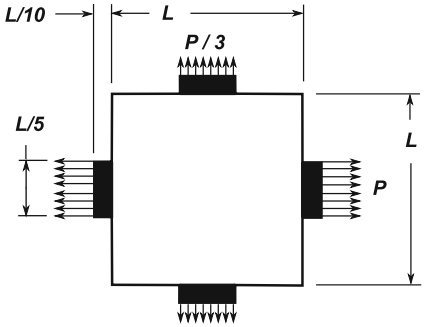

Fig. 8 Two phase bi-axially loaded plate problem

3.2 Interface condition

Using a Heaviside enrichment (11) bypasses the issues of the kink enrichment and can represent more general jump discontinuities that are common in, for example, displacements across cracks and temperature fields at small scales across material interfaces; see, for example, Maute et al. (2011). However, since the Heaviside enrichment does not inherently satisfy the displacement continuity condition, the weak form (7) needs to be augmented to enforce the continuity conditions at the phase boundaries.

Common formulations to enforce the continuity of the physical response across phase boundaries in the XFEM include stabilized Lagrange multiplier methods and the Nitsche method. These methods are discussed in detail by Stenberg (1995), Juntunen and Stenberg (2009), and Dolbow and Harari (2009). The standard Lagrange multiplier approach is not suitable for the XFEM as it suffers from stability issues. Here we enforce the displacement continuity along $\Gamma_{A,B}$ by the stabilized Lagrange multiplier method and augment the residual (7) as follows:

$$\tilde{W} = W - \int_{\Gamma_{A,B}} [\mathbf{v}] \cdot \boldsymbol{\lambda}\, d\Gamma_{A,B} - \gamma \int_{\Gamma_{A,B}} \boldsymbol{\mu} \cdot [\mathbf{u}] d\Gamma_{A,B} + \int_{\Gamma_{A,B}} \boldsymbol{\mu} \cdot \left(\boldsymbol{\lambda} - \bar{\boldsymbol{\sigma}} \cdot \mathbf{n}_{A,B}\right) d\Gamma_{A,B}, \tag{13}$$

$$[\mathbf{u}] = \mathbf{u}^{(A)} - \mathbf{u}^{(B)}\,, [\mathbf{v}] = \mathbf{v}^{(A)} - \mathbf{v}^{(B)}, \tag{14}$$

Table 1 Parameters for beam problem

Length of design domain	$L = 3\ m$
Elastic modulus	$E = 1\ Pa$
Poisson's ratio	$\nu = 0.2$
Spring constant	$k = 10^{-7}\ N/m$
Point load	$P = 1\ N$
Thickness	$t = 1\ m$
Maximum area	$\bar{V}_A = 3\ m^3$
Element size	$\Delta x = 0.05\ m$
Convergence Criteria	$\Delta\mathcal{F} = 2.0e^{-5}$

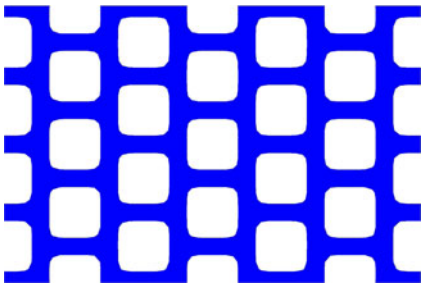

Fig. 9 Initial design for cantilevered beam problem

$$\bar{\boldsymbol{\sigma}} = \frac{1}{2}\left(\boldsymbol{\sigma}^{(A)} + \boldsymbol{\sigma}^{(B)}\right), \tag{15}$$

where $\boldsymbol{\lambda}$ is the Lagrange multiplier and $\boldsymbol{\mu}$ is the associated test function. The operator $[\cdot]$ denotes the jump between corresponding quantities across the phase boundary. The above formulation can be derived from the interface contribution (8) and the assumption that the stress tensor $\bar{\boldsymbol{\sigma}}$ at the interface can be approximated by (15). Note the third term in (13) stabilizes the formulation by enforcing weakly the compatibility between the Lagrange multiplier and the traction $\bar{\boldsymbol{\sigma}} \cdot \mathbf{n}_{A,B}$. The higher the weight γ the more accurately the interface condition is satisfied at the cost of numerical stability. In the numerical studies below we use a constant approximation of the Lagrange multiplier along an elemental interface. For computational efficiency, the Lagrange multipliers are solved for at the element level and condensed out from the global residual equations.

For the case where the second phase is void, no displacement continuity condition needs to be enforced. If an external load $\mathbf{f}_{A,B}$ is acting on the phase boundary the following integral is added to the residual (7):

$$\tilde{W} = W - \int_{\Gamma_{A,B}} \mathbf{v} \cdot \mathbf{f}_{A,B}\, d\Gamma_{A,B}. \tag{16}$$

If the phase boundary is traction free, there are no contributions to the residual equations.

4 Numerical examples

The generalized XFEM formulation is studied with two numerical problems: a) a cantilevered beam shown in Fig. 7, and b) a bi-axially loaded, two-material plate shown in Fig. 8. These examples show the deficiencies of the simplified enrichment strategy and the generality of the presented method.

In both examples, the objective is to minimize the compliance augmented by a penalty on the perimeter of the structure:

$$\mathcal{F} = \int_{\Gamma_N} \mathbf{f} \cdot \mathbf{u}\, d\Gamma_N + p \int_{\Gamma_{A,B}} d\Gamma_{A,B}, \tag{17}$$

where p is a penalty parameter. As previously shown by Allaire et al. (2004), Maute et al. (2011), and van Dijk et al. (2012) the penalty on the perimeter regularizes the problem and prevents the emergence of small geometric features. We further constrain the volume of the stiffer phase, here phase "A", to suppress trivial solutions:

$$\mathcal{G} = \frac{1}{\overline{V}_A} \int_{\Omega_A} d\Omega - 1 \leq 0, \tag{18}$$

where $\overline{V}_A$ is the maximum allowable volume of phase "A". The design domain is discretized by a uniform mesh with bi-linear finite elements. The element sizes are reported with the optimization results for each problem. Each non-intersected element is integrated with 2×2 Gauss quadrature and intersected elements are integrated with 7 - point Gauss quadrature in each triangle. The level set field may lead to intersections with small areas over which a degree of freedom interpolates the displacement fields. As these areas approach zero, the finite element problem suffers from ill - conditioning. To mitigate this issue we employ the pre - conditioning scheme of Lang et al. (2013). The resulting linear system is solved by a direct solver. The design sensitivities are computed by the adjoint method. The Jacobian of the state equation (13) and the partial derivatives of the compliance with respect to the state variables are evaluated based on the analytically differentiated formulations. The partial derivatives of elemental residuals and the derivatives of the perimeter and volume with respect to the nodal level set values are evaluated by finite differencing. Note the computational cost of the finite difference operations is insignificant as only nodal level set values that belong to intersected elements need to be considered.

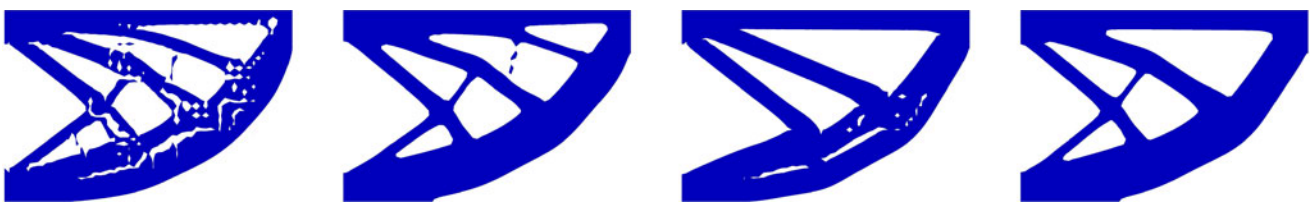

(a) Standard enrich., $p = 0.0$. (b) Standard enrich., $p = 0.2$. (c) Consistent enrich., $p = 0.0$. (d) Consistent enrich., $p = 0.2$.

Fig. 10 Optimization results of cantilevered beam problem with $r = 0.07501\ m$ and varying enrichment strategies and perimeter penalties, p

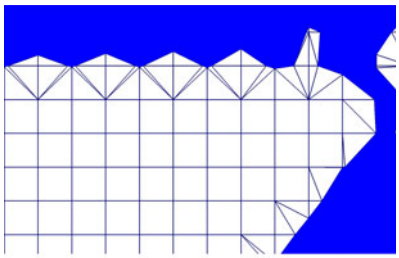

(a) Material layout with artificially high stiffness.

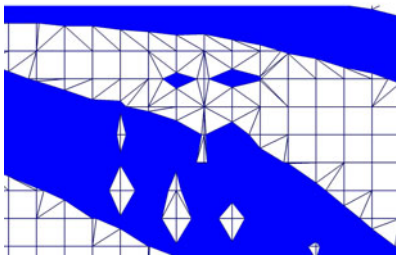

(b) Free floating material.

Fig. 11 Deficiencies of standard enrichment method

The optimization problems are solved by the Globally Convergent Method of Moving Asymptotes (GCMMA) of Svanberg (2002). The GCMMA constructs a sequence of convex separable sub-problems that are solved by a primal-dual method, and is guaranteed to converge to a Karush-Kuhn-Tucker optimal point. This algorithm is specifically suited for non-linear optimization problems with a large number of design variables and few non-linear constraints.

4.1 Cantilevered beam

The two dimensional cantilevered beam problem of Fig. 7 is optimized with the material and optimization parameters summarized in Table 1. Note phase "B" is void.

4.1.1 Effect of consistent enrichments

As shown in Section 3.1.1, using an inconsistent enrichment for disconnected phases may over-predict the local stiffness of the material layout and introduce numerical artifacts. The results shown in this section illustrate the effect of this deficiency on the optimized design. For all results presented in this sub-section, the design domain is initialized with an array of 7×4 holes, shown in Fig. 9.

First, we apply a filter of $r = 0.07501\ m$ and study the influence of the enrichment strategy for perimeter penalty factors of $p = 0.0$ and $p = 0.2$. As the results in Fig. 10 show, the over-prediction of stiffness in the standard enrichment scheme leads to material layouts with numerical artifacts in the design. The formation of diamond-shaped inclusions resembles the well-known "checker-board" patterns observed in density methods when low-order elements and no filtering or perimeter penalty is applied; see, for example, Sigmund and Petersson (1998). In addition, the standard enrichment strategy promotes the formation of free floating material.

Figure 11 shows close-up views of Fig. 10a. The triangulated mesh is shown to illustrate the elemental connectivity over the "void" phase. Using the standard enrichment strategy, diamond-shaped structures have an artificially large stiffness with a small volume of material, and free floating features are stiffened through artificial coupling of disconnected material. Using the standard enrichment approach and a perimeter penalty of $p = 0.2$ removes many of the numerical artifacts, but does not eliminate them, see Fig. 10b.

The consistent enrichment with $p = 0.0$ has significantly less numerical artifacts compared to the standard enrichment. These artifacts are caused by not sufficiently resolving the structural response of small geometric features, an issue that is common to all finite element schemes used in topology optimization. To mitigate this issue the local feature size needs to be controlled. In the absence of local control techniques for level set methods, here we employ a perimeter penalty. While penalizing (or constraining) the perimeter is not guaranteed to prevent the emergence of small local features, for this problem the combination of perimeter penalty and consistent enrichment leads to a physically reasonable design, see Fig. 10d.

4.1.2 Filtering

In general, level set optimization methods suffer from slow convergence; see, for example, van Dijk et al. (2013). The

(a) no filter, 594 iterations. (b) $r = 0.07501\ m$, 415 iterations. (c) $r = 0.15001\ m$, 287 iterations.

Fig. 12 Effect of filter radius on the optimized design for $p = 0.2$

Table 2 Convergence of the optimization process

Filter radius [m]	Number of iterations	Compliance
no filter	594	37.3721
$r = 0.07501$	415	37.5542
$r = 0.15001$	287	37.9047

convergence rate is affected by the localization of the design sensitivities and is independent of whether Hamilton-Jacobi schemes or mathematical programming methods are used to update the design. That is, the gradients of the objective and constraints with respect to the nodal level set values are zero, except for the ones that influence the zero level set contour. de Ruiter and van Keulen (2004), Wang and Wang (2006a), and Pingen et al. (2010) mitigate this issue by interpolating the level-set field with shape functions that have a non-local support, such as radial-basis functions. Alternatively, the level set field can be smoothed by the linear filter (3). As the filter radius, r, increases the zone of influence is broadened and the convergence of the optimization process is accelerated. We study the effect of the linear filter on the beam problem of Fig. 7.

First we consider a perimeter penalty of $p = 0.2$. The optimized designs not using a filter and for a filter radius of 0.07501 m and 0.15001 m are shown in Fig. 12. In Table 2, the number of iterations needed to obtain a converged design and the compliance value of the final design are listed in dependence of the filter radius. The convergence is accelerated with a larger filter radius. However, larger filter radii tend to lose design features. This is due in part to more rapid design changes in the optimization process, which tend to "skip over" designs with small features. The loss of features is also due to the filter smoothing out the level set field over a large "void" area, often but not necessarily causing small features to disappear.

Filtering the design variables or the sensitivities is typically sufficient to regularize problems solved by density methods; see, for example, Sigmund (2009). To demonstrate that filtering of level set fields does not provide a similar regularization effect, we solve the beam problem for several filter radii without penalizing the perimeter, i.e. $p = 0.0$. Figure 13 shows the optimized designs. While the convergence is accelerated similarly to the $p = 0.2$ case, smoothing the level set field cannot suppress the emergence of small features. In this example the filter removes small oscillations in the geometry, as seen in Fig. 13a versus Fig. 13b. In general, however, the filter does not necessarily lead to smooth shapes, although it is our experience that it often does in practice as shown in the examples presented above.

Table 3 Parameters for bi-axially loaded plate problem

Length and width of design domain	$L = 4.0\ m$
Elastic modulus of material "A"	$E_A = 1.0\ Pa$
Poisson's ratio of material "A" and "B"	$\nu = 0.2$
Vertical distributed load	$P_v = 80.0\ N/m$
Horizontal distributed load	$P_h = 240.0\ N/m$
Thickness	$t = 1\ m$
Maximum area of phase "A"	$\bar{V}_A = 4\ m^3$
Filter radius	$r = 0.06\ m$
Perimeter penalty	$p = 0.001$
Element size	$\Delta x = 0.05\ m$

4.2 Two phase optimization

In the cantilevered beam problem of Section 4.1, we studied the proposed XFEM approach for analyzing problems where one of the phases is void. This configuration does not require enforcing the displacement continuity condition (13) along the phase boundary. In this section we study an optimization problem where both phases represent an elastic material with finite stiffness. These types of problems amplify the need for a proper enrichment strategy and require satisfying the displacement continuity condition along phase boundaries.

We consider a bi-axially loaded plate with the material properties and optimization parameters summarized in Table 3. The small rectangular areas at which the loads are acting are not part of the design domain and are occupied by the stiff phase. The compliance of the plate is optimized for three stiffness ratios of the materials: the elastic modulus of phase "B" is taken to be $E_B = 10^{-1}E_A$, $E_B = 10^{-2}E_A$, and $E_B = 10^{-4}E_A$.

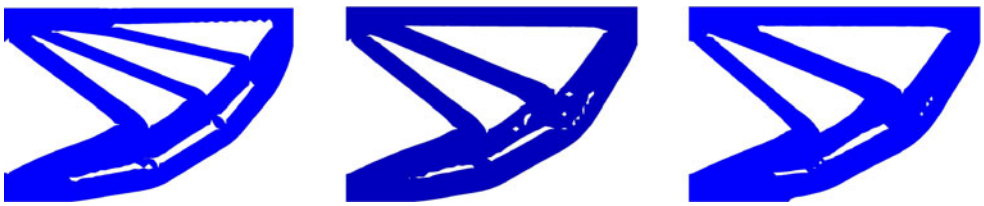

(a) no filter. (b) $r = 0.07501\ m$. (c) $r = 0.15001\ m$.

Fig. 13 Effect of the filter radius on the optimized design for $p = 0.0$

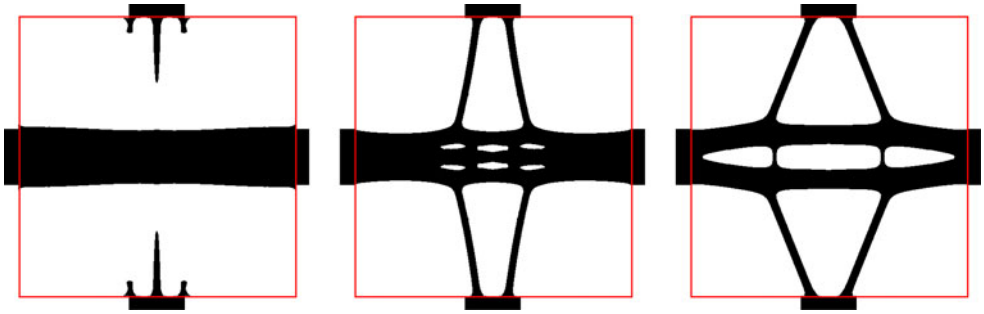

(a) $E_B = 10^{-1}E_A$. (b) $E_B = 10^{-2}E_A$. (c) $E_B = 10^{-4}E_A$.

Fig. 14 Optimized designs of the bi-axially loaded plate: black – stiff phase, white – soft phase

The optimized designs for the three stiffness ratios are shown in Fig. 14. For $E_B = 10^{-1}E_A$ the compliance in the vertical direction remains small and phase "A" is placed to stiffen the structure in the horizontal direction. As phase "B" becomes softer the compliance in the vertical direction becomes more important and the optimized design uses increasingly more of material "A" to stiffen the vertical direction.

The cross comparison of the three designs is shown in Table 4. The lowest compliance is obtained with the elastic modulus combination that each design was optimized for, as expected. For a large stiffness of phase "B", the variance in the compliance of the optimized designs is low as the elastic moduli of two phases are similar and the compliance is less sensitive to the material layout. In the case the stiffness of phase "B" is much lower than the one of phase "A", the compliance strongly depends on the material layout.

5 Conclusions

A generalized formulation of the eXtended Finite Element Method has been studied for solving level set topology optimization problems. Departing from simplified and potentially inaccurate enrichment strategies frequently used in topology optimization, we have presented a generalized Heaviside enrichment strategy that consistently interpolates state variables for complex geometries without the need for adaptively refining the mesh. A stabilized Lagrange multiplier method was used to enforce continuity conditions along phase boundaries. We have added soft springs to the computational model to bypass ill - conditioning issues due to free-floating material. We have studied "material-void" and "material-material" optimization problems to evaluate the proposed XFEM framework.

The XFEM formulation presented in this paper is robust and efficient in analyzing geometrically complex configurations, which often emerge in topology optimization. In contrast to standard enrichment methods, the generalized enrichment strategy does not over-predict the stiffness of small geometric features and prevents the formation of "checker-board"-like numerical artifacts. Heaviside enrichment functions provide great flexibility in handling a broad class of physical problems, but may require enforcing additional continuity conditions across the phase boundaries. In this study, continuity constraints in the displacement field are enforced by a stabilized Lagrange multiplier method. For "material-void" problems, elements entirely in the "void" phase are omitted in the element assembly process and the degrees of freedom that interpolate the "void" phase are eliminated from the system of equations; both techniques reduce the computational cost of solving the XFEM problem. While the extension of our XFEM formulation to three dimensions is straight forward, an efficient and robust implementation is not trivial and is currently being studied.

In this paper we have applied a perimeter constraint to suppress small geometric features in the optimized design. While this approach was successful for the compliance problems studied, constraining the perimeter does not provide a local geometry control. Furthermore, we showed that, in contrast to density methods, smoothing the level set field is insufficient to regularize the optimization problem, but it improves the convergence of the optimization process. These observations are in agreement with the findings of van Dijk et al. (2013) and Sigmund and Maute (2013) for level set methods using Ersatz material and emphasize the

Table 4 Cross comparison of compliance for the optimized designs for different E_A/E_B ratios

Case	$E_A/E_B = 10^1$	$E_A/E_B = 10^2$	$E_A/E_B = 10^4$
Optimized for $E_A/E_B = 10^1$	0.24318	0.72295	49.11647
Optimized for $E_A/E_B = 10^2$	0.24567	0.30205	0.32164
Optimized for $E_A/E_B = 10^4$	0.24500	0.30648	0.31282

need for regularization techniques with local shape control in level set topology optimization.

Acknowledgments The author acknowledges the support of the National Science Foundation under grants EFRI-SEED–1038305 and CMMI–1201207. The opinions and conclusions presented in this paper are those of the authors and do not necessarily reflect the views of the sponsoring organization.

References

Allaire G, Jouve F, Toader AM (2004) Structural optimization using sensitivity analysis and a level-set method. J Comput Phys 194(1):363–393

Babuška I, Melenk JM (1997) The partition of unity method. Int J Numer Methods Eng 40(4):727–758

Bendsøe M (1989) Optimal shape design as a material distribution problem. Struct Multidiscip Optim 1(4):193–202

Bendsøe M, Kikuchi N (1988) Generating optimal topologies in structural design using a homogenization method. Comput Methods Appl Mech Eng 71(2):197–224

Bendsøe MP, Sigmund O (2003) Topology optimization: theory, methods and applications. Springer

Burger M, Osher SJ (2005) A survey in mathematics for industry a survey on level set methods for inverse problems and optimal design. Eur J Appl Math 16:263–301

de Ruiter M, van Keulen F (2000) Topology optimization: approaching the material distribution problem using a topological function description. In: Topping BHV (ed) Computational Techniques for Materials, Composites and Composite Structures, Edinburgh, pp 111–119

de Ruiter MJ, van Keulen F (2004) Topology optimization using a topology description function. Struct Multidiscip Optim 26(6):406–416

Daux C, Moes N, Dolbow J, Sukumark N, Belytschko T (2000) Arbitrary branched and intersecting cracks with the extended finite element method. Int J Numer Method Eng 48:1741–1760

Dolbow J, Harari I (2009) An efficient finite element method for embedded interface problems. Int J Numer Method Eng 78:229–252

Duysinx P, Miegroet L, Jacobs T, Fleury C (2006) Generalized shape optimization using x-fem and level set methods. In: IUTAM Symposium on Topological Design Optimization of Structures, Machines and Materials, Springer, pp 23–32

Fish J (1992) The s-version of the finite element method. Comput Struct 43(3):539–547

Fries T, Belytschko T (2010) The extended/generalized finite element method: an overview of the method and its applications. Int J Numer Methods Eng 84(3):253–304

Fries TP (2008) A corrected xfem approximation without problems in blending elements. Int J Numer Methods Eng 75(5):503–532

Fries TP (2009) The intrinsic xfem for two-fluid flows. Int J Numer Meth Fluids 60(4):437–471

Gerstenberger A, Wall WA (2008) An extended finite element method/Lagrange multiplier based approach for fluid-structure interaction. Comput Methods Appl Mech Eng 197:1699–1714

Guest J (2009) Topology optimization with multiple phase projection. Comput Methods Appl Mech Eng 199(1-4):123–135

Haber R, Bendsøe M (1998) Problem formulation, solution procedures and geometric modeling: key issues in variable-topology optimization. In: AIAA/USAF/NASA/ISSMO Symposium on Multidisciplinary Analysis and Optimization, AIAA, no. AIAA-1998-4948 in Collection of Technical Papers. Pt. 3

Hansbo A, Hansbo P (2004) A finite element method for the simulation of strong and weak discontinuities in solid mechanics. Comput Methods Appl Mech Eng 193(33–35):3523–3540

Juntunen M, Stenberg R (2009) Nitsche's method for general boundary conditions. Math Comput 78:1353–1374

Kreissl S, Maute K (2011) Topology optimization for unsteady flow. Int J Numer Methods Eng 87:1229–1253

Kreissl S, Maute K (2012) Levelset based fluid topology optimization using the extended finite element method. Struct Multidiscip Optim 46(3):311–326

Lang C, Makhija D, Doostan A, Maute K (2013) A simple and efficient projection scheme for heaviside enriched xfem. Submitted to Computational Mechanics

Luo Z, Tong L, Wang MY, Wang S (2007) Shape and topology optimization of compliant mechanisms using a parameterization level set method. J Comput Phys 227(1):680–705

Maute K, Ramm E (1995) Adaptive topology optimization. Struct Multidiscip Optim 10(2):100–112

Maute K, Ramm E (1997) Adaptive topology optimization of shell structures. AIAA J 35(11):1767–1773

Maute K, Schwarz S, Ramm E (1998) Adaptive topology optimization of elastoplastic structures. Struct Multidiscip Optim 15(2):81–91

Maute K, Kreissl S, Makhija D, Yang R (2011) Topology optimization of heat conduction in nano-composites. In: 9th World Congress on Structural and Multidisciplinary Optimization, Shizuoka

Osher SJ, Sethian JA (1988) Fronts propagating with curvature dependent speed: algorithms based on Hamilton-Jacobi formulations. J Comput Phys 79:12–49

Pingen G, Waidmann M, Evgrafov A, Maute K (2010) A parametric level-set approach for topology optimization of flow domains. Struct Multidiscip Optim 41(1):117–131

Schleupen A, Maute K, Ramm E (2000) Adaptive fe-procedures in shape optimization. Struct Multidiscip Optim 19:282–302

Sethian J, Wiegmann A (2000) Structural boundary design via level set and immersed interface methods. J Comput Phys 163(2):489–528

Sigmund O (2009) Manufacturing tolerant topology optimization. Acta Mech Sinica/Lixue Xuebao 25(2):227–239

Sigmund O, Maute K (2012) Sensitivity filtering from a continuum mechanics perspective. Struct Multidiscip Optim 1–5

Sigmund O, Maute K (2013) Topology optimization approaches: a comparative review. Structural and Multidisciplinary Optimization doi:10.1007/s00158-013-0978-6

Sigmund O, Petersson J (1998) Numerical instabilities in topology optimization: a survey on procedures dealing with checkerboards, mesh-dependencies and local minima. Struct Multidiscip Optim 16(1):168–75

Stenberg R (1995) On some techniques for approximating boundary conditions in the finite element method. J Comput Appl Math 63(1–3):139–148

Svanberg K (2002) A class of globally convergent optimization methods based on conservative convex separable approximations. SIAM J Optim 12:555–573

Terada K, Asai M, Yamagishi M (2003) Finite cover method for linear and non-linear analyses of heterogeneous solids. Int J Numer Methods Eng 58(9):1321–1346. doi:10.1002/nme.820

van Dijk N, Langelaar M, van Keulen F (2012) Explicit level-set-based topology optimization using an exact heaviside function and consistent sensitivity analysis. Int J Numer Methods Eng 91(1):67–97

van Dijk N, Maute K, Langelaar M, Keulen F (2013) Level-set methods for structural topology optimization: a review. Struct Multidiscip Optim pp 1–36

van Miegroet L, Duysinx P (2007) Stress concentration minimization of 2d filets using x-fem and level set description. Struct Multidiscip Optim 33(4–5):425–438

van Miegroet L, Moës N, Fleury C, Duysinx P (2005) Generalized shape optimization based on the level set method. In: 6th World Congress of Structural and Multidisciplinary Optimization

Wang F, Lazarov BS, Sigmund O (2011) On projection methods, convergence and robust formulations in topology optimization. Struct Multidiscip Optim 43(6):767–784

Wang MY, Wang X, Guo D (2003) A level set method for structural topology optimization. Comput Methods Appl Mech Eng 192(1–2):227–246. doi:10.1016/S0045-7825(02)00559-5

Wang S, Wang MY (2006a) Radial basis functions and level set method for structural topology optimization. Int J Numer Methods Eng 65(12):2060–2090

Wang S, Wang MY (2006b) A moving superimposed finite element method for structural topology optimization. Int J Numer Meth Eng 65:1892–1922

Wei P, Wang M, Xing X (2010) A study on X-FEM in continuum structural optimization using a level set model. Comput-Aided Des 42(8):708–719

Wilke DN, Kok S, Groenwold AA (2006) A quadratically convergent unstructured remeshing strategy for shape optimization. Int J Numer Methods Eng 65(1):1–17

Xia Q, Shi T, Liu S, Wang MY (2012) A level set solution to the stress-based structural shape and topology optimization. Comput Struct 90–91:55–64

Yamada T, Izui K, Nishiwaki S, Takezawa A (2010) A topology optimization method based on the level set method incorporating a fictitious interface energy. Comput Methods Appl Mech Eng 199(45–48):2876–2891

Zhou M, Rozvany GIN (1991) The COC algorithm, part II: topological, geometrical and generalized shape optimization. Comput Methods Appl Mech Eng 89(1–3):309–336